8626 *Biochemistry* **2010,** *49,* 8626–8635
DOI: 10.1021/bi101015p

BIOCHEMISTRY
including biophysical chemistry & molecular biology
Article

The Protein-Free IANUS Peptide Array Uncovers Interaction Sites between *Escherichia coli* Parvulin 10 and Alkyl Hydroperoxide Reductase[†]

Miroslav Malešević,[‡] Angela Poehlmann,[‡,∥] Birte Hernandez Alvarez,[‡,⊥] André Diessner,[§] Mario Träger,[‡] Jens-Ulrich Rahfeld,[‡,@] Günther Jahreis,[‡] Sandra Liebscher,[§] Frank Bordusa,[§] Gunter Fischer,*[,‡] and Christian Lücke*[,‡]

[‡]*Max Planck Research Unit for Enzymology of Protein Folding, Weinbergweg 22, 06120 Halle/Saale, Germany, and* [§]*Institute of Biochemistry and Biotechnology, Martin Luther University Halle-Wittenberg, Kurt-Mothes-Straße 3, 06120 Halle/Saale, Germany.* [∥]*Present address: Institute of Pathology, Otto-v.-Guericke University, Leipziger Str. 44, 39120 Magdeburg, Germany.* [⊥]*Present address: Max Planck Institute for Developmental Biology, Spemannstr. 35−39, 72076 Tübingen, Germany.* [@]*Present address: Probiodrug AG, Weinbergweg 22, 06120 Halle/Saale, Germany.*

Received June 24, 2010; Revised Manuscript Received August 26, 2010

ABSTRACT: The reliable identification of interacting structural elements without prior isolation of interacting proteins can be achieved by using the novel fluorescence resonance energy transfer-coupled IANUS (Induced orgANization of strUcture by matrix-assisted togethernesS) peptide array. Here we report that parvulin 10 (Par10), an abundant *Escherichia coli* peptidyl prolyl *cis*/*trans* isomerase (PPIase), physically interacts with the alkyl hydroperoxide reductase subunit C (AhpC) in bacterial cell extracts, as determined by affinity chromatography and chemical cross-linking experiments. A Par10-negative *E. coli* strain showed increased sensitivity toward hydrogen peroxide compared to the wild-type strain. The IANUS experiment revealed three segments of the peroxiredoxin AhpC chain as potential Par10 binding partners. Inhibition of the Par10 PPIase activity by the corresponding AhpC-derived peptides as well as NMR data of ^{15}N-labeled Par10 in the presence of the AhpC$^{115-132}$ peptide or full-length AhpC confirmed that the putative Par10 active site is involved in the Par10−AhpC interaction. Moreover, NMR-based docking calculations as well as NOESY exchange peaks between the proline *cis* and *trans* isomers revealed the Asp125-Pro126 moiety of the AhpC segment G115−A132 as a substrate for Par10 enzymatic action. On the basis of these data, we conclude that Par10 catalytic activity is involved in the cellular protection against oxidative stress.

Peptide arrays prepared by spot synthesis on different solid carriers are powerful tools for the study of protein−protein and protein−ligand interactions (*1*, *2*). Such arrays, in which peptides or members of any other compound class are synthesized simultaneously and in parallel at distinct positions on a solid carrier, have found manyfold applications in biological and pharmaceutical research (*3*, *4*). However, the use of native proteins for the interaction assay probes is a prerequisite that becomes the main obstacle when utilizing these arrays. The recently developed IANUS[1] (Induced orgANization of strUcture by matrix-assisted togethernesS) peptide array has the potential to evolve into a protein-free method for detection of protein binding sites (*5*). This array is designed to reveal the architecture of protein−protein interaction surfaces through template-assisted intramolecular peptide−peptide interactions.

Peptidyl-prolyl *cis*/*trans* isomerases (PPIases), such as parvulins (Par), cyclophilins (Cyp), and FK-506 binding proteins (FKBP), are folding-helper enzymes that have evolved to catalyze the *cis*−*trans* isomerization of prolyl imide bonds (*6*, *7*). The peptide bond isomerization catalyzed by PPIases occurs in many fundamental biological processes like in vivo protein folding (*8*, *9*). PPIases have also been associated with various cell signaling processes, such as the regulation of the mitochondrial permeability transition pore implicated in mitochondrion-mediated apoptosis. Moreover, the involvement of certain PPIases in various stress-dependent cellular mechanisms has been reported. While *Vicia faba* cyclophilin Cyp21 and FKBP13, for instance, feature light-dependent expression, it has been reported that Cyp18, Cyp20, and FKBP13 from yeast can be induced by heat shock (*10*, *11*). Moreover, an elevated expression level after accumulation of misfolded proteins was shown for the periplasmic folding catalyst FKBP26 and the parvulin homologues Par47 and Par68 in *Escherichia coli* (*12*, *13*). The direct involvement of cyclophilins in the adapting cellular response was also demonstrated in vertebrate cells showing increased sensitivity toward oxidative stress factors after cyclosporine A treatment (*14*). Mammalian Cyp18 provides protection against peroxide-induced cell death in vertebrate cells because of its PPIase activity (*15*, *16*). Furthermore, it was reported that the bacterial PPIase RopA regulates acid and oxidative stress tolerance in *Streptococcus mutans* (*16*).

[†]This work was supported by the Deutsche Forschungsgemeinschaft (SFB 610).

*To whom correspondence should be addressed. E-mail: Fischer@enzyme-halle.mpg.de or Luecke@enzyme-halle.mpg.de. Phone: +49-345-5522801. Fax: +49-345-5511972.

[1]Abbreviations: Abz, aminobenzoyl; AhpC, alkyl hydroperoxide reductase subunit C; AhpF, alkyl hydroperoxide reductase FAD-binding subunit; AIRs, ambiguous interaction restraints; CFU, colony-forming units; CSP, chemical shift perturbation; Cyp, cyclophilins; DCM, dichloromethane; DIPEA, *N*,*N*-diisopropylethylamine; DMF, dimethylformamide; DMP, dimethylpimelimidate; DTT, dithiothreitol; FKBP, FK-506 binding proteins; FRET, fluorescence resonance energy transfer; GST, glutathione *S*-transferase; IANUS, Induced orgANization of strUcture by matrix-assisted togethernesS; Par10, parvulin 10; pNa, *p*-nitroanilide; PPIase, peptidyl prolyl *cis*/*trans* isomerase; PyBOP, benzotriazol-1-yloxytris(pyrrolidino)phosphonium hexafluorophosphate; TFE, trifluoroethanol.

 Published on Web 08/31/2010

Par10 is the first described and smallest known PPIase (*17*, *18*), consisting of 92 amino acids with a molecular mass of 10.1 kDa. It is located in the cytosol of *E. coli*, but the physiological role of this enzyme still remains to be elucidated. Juglon (5-hydroxy-1,4-naphthochinone), which binds irreversibly to several parvulins (*19*), is the only known natural Par10 inhibitor, while no protein interaction partners of Par10 have been published to date.

Here, for the first time, a cellular interaction partner of Par10, namely alkyl hydroperoxide reductase subunit C (AhpC), has been identified. Moreover, peptides corresponding to AhpC segments R31−V45, S85−D98, and G115−A132 were identified by the IANUS peptide array as AhpC interaction interfaces for Par10. Subsequent NMR measurements and docking calculations revealed that the peptide derived from AhpC segment G115−A132 binds to the Par10 binding pocket and acts as a substrate. Moreover, the first evidence that the interaction of Par10 with the peroxiredoxin AhpC influences the oxidative stress response in bacterial cells is also presented.

MATERIALS AND METHODS

Cloning and Overexpression of a Glutathione S-Transferase−Par10 Fusion Protein. A *parA* DNA fragment was cloned into the pGEX-5x-1 vector (Pharmacia). The recombinant plasmid was transformed in competent *E. coli* JM109 cells. For the expression of the recombinant GST−Par10 fusion protein, a 1 L culture of transformed cells was grown to an optical density of A_{600} = 0.5 at 37 °C, induced with 1 mM isopropyl β-D-1-thiogalactopyranoside, and grown for an additional 5 h. Overexpression of GST protein was performed under the same conditions after the transformation of the unmodified pGEX-5x-1 plasmid in JM109 cells.

Affinity Purification of a 22 kDa Par10 Binding Protein. The *E. coli* overexpression culture of the GST−Par10 fusion protein was pelleted by centrifugation. Cells were resuspended in 10 mM phosphate buffer [150 mM NaCl and 2 mM dithiothreitol (DTT) (pH 7.5)], French pressed three times, and ultracentrifuged after addition of 0.01% (v/v) Benzonase. The supernatant was passed through a glutathione Sepharose B column (1 cm × 3 cm, Pharmacia) that had been equilibrated with the phosphate buffer mentioned above. The fusion protein bound specifically to the column material. After being washed with 50 mL of application buffer, tightly bound proteins were eluted with a linear gradient from 0 to 2 M NaCl in phosphate buffer. The GST−Par10 fusion protein was recovered by elution with 10 mM phosphate buffer (pH 7.5) containing 5 mM reduced glutathione. Proteins were resolved by SDS−PAGE and detected by silver or Coomassie Blue staining.

Chemical Cross-Linking. *E. coli* Par10, His_6-AhpC, and His_6-AhpF were prepared as described in the Supporting Information. The corresponding proteins (15 μmol) were mixed in a final volume of 100 μL of sodium phosphate buffer (0.1 M, pH 9.1) and 1 mM dimethylpimelimidate (DMP). The mixtures were incubated with occasional shaking for 1 h at 25 °C. Subsequently, SDS sample buffer (40 μL) was added, and the samples were analyzed by SDS−PAGE followed by silver staining or Western blot analysis using the Fast Blot B32 semidry electroblotting system (Biometra, Göttingen, Germany).

IANUS Peptide Array. The trifunctional orthogonally protected linker **1** was synthesized as described previously (*20*). Two β-Ala residues were used for a Whatman 540 (Whatman, Dassel, Germany) cellulose membrane derivatization and spot definition (*21*). Template **1** was preactivated with 1 equiv of benzotriazol-1-yloxytris(pyrrolidino)phosphonium hexafluorophosphate (PyBOP) and 3 equiv of *N*,*N*-diisopropylethylamine (DIPEA) and subsequently coupled to all spots. Overlapping 12-mer peptides spanning the entire AhpC sequence with a frame shift of two amino acids (i.e., 88 spots) were synthesized with the autospot robot ASP-222 (Abimed) using the standard protocol for spot synthesis (*21*). Fmoc-protected amino acids were preactivated as pentafluorophenyl esters. Acetic anhydride was used for capping the remaining uncoupled N-terminal amino groups. In each synthesis cycle, the Fmoc protection was removed with a 20% piperidine solution in dimethylformamide (DMF). Afterward, an additional β-Ala residue was coupled to the N-termini of all peptides, followed by coupling of 5(6)-carboxyfluorescein, which was preactivated with 1 equiv of PYBOP and 3 equiv of DIPEA. After cleavage of the Aloc protective group with Pd-$(PPh_3)_4$ and phenylsilane in degassed dichloromethane (DCM) under an argon atmosphere, the LGEFRQGQMVPAF peptide was synthesized stepwise into all 88 spots using to the protocol described above. Finally, dansyl chloride in the presence of 1 equiv of DIPEA in DMF was coupled to the peptide N-terminus, and all side chain protecting groups were removed by a 3 h treatment with a 50% TFA/DCM mixture. For the peptide pair combination in each spot, see Table S1 of the Supporting Information.

After the membrane had been washed with DCM (three times), DMF (three times), MeOH (three times), and 30 mM phosphate buffer (pH 7.5) (three times), the fluorescence was recorded using the DIANA chemiluminescence detection system (Raytest, Straubenhardt, Germany). The membrane was wetted with phosphate buffer and irradiated with 312 nm UV light. Emission light was filtered with a "Sybr green" filter (510−530 nm). The densitometric analysis of spot intensities was performed using AIDA version 2.0.

PPIase Activity Measurements. Par10 PPIase activity was determined at 10 °C by applying a protease-free assay in 35 mM HEPES buffer (pH 7.8) containing 1 μM bovine serum albumin. A 1 mM stock solution of substrate **10** was prepared in 0.5 M LiCl in trifluoroethanol (TFE). The reaction was started by the addition of 1.6 μL of the substrate solution to the reaction mixture (end volume of 800 μL). For inhibition studies, peptides **2**−**9** (1 mM stock solutions) were added to the reaction mixture containing 1.9 nM Par10. For peptides with low solubility in this buffer, a saturated solution was prepared. The peptide concentrations were calculated from the absorbance at 280 nm after centrifugation. If peptides had no Tyr or Trp residues in the sequence, the concentration was determined by weighting. A Hitachi F-3010 fluorescence spectrophotometer was used for monitoring the time course of the first-order reaction. The sample was irradiated with UV light at 320 nm and the resulting time-dependent fluorescence filtered at 420 nm. Each experiment was repeated twice and the average value calculated.

Collection and Analysis of NMR Data. The NMR samples all contained 0.5 mM ^{15}N-labeled *E. coli* Par10 in 10 mM potassium phosphate buffer [100 mM KCl and 1 mM DTT (pH 7.25)]. The ^{15}N-labeled Par10 was prepared as described in the Supporting Information. For chemical shift perturbation (CSP) mapping, samples of ^{15}N-labeled Par10 were supplemented with a 2-fold excess of peptide **7** or a 3-fold excess of His_6-AhpC. All NMR spectra were recorded at 25 °C using a Bruker DRX 500 spectrometer operating at a 500.13 MHz proton resonance frequency and equipped with a 5 mm triple-resonance

probe featuring XYZ-gradient capability. Homonuclear two-dimensional (2D) NOESY and heteronuclear 2D $^{1}H-^{15}N$ HSQC experiments were performed with the carrier placed in the center of the spectrum on the water resonance, which was suppressed by applying a WATERGATE sequence. Quadrature detection in the indirectly detected dimension was obtained by the States−TPPI method. All NMR spectra were recorded and processed on Silicon Graphics computers using XWINNMR version 3.5 (Bruker Bio-Spin, Rheinstetten, Germany). A 90° phase-shifted squared sine-bell function was used for apodization in all dimensions. Polynomial baseline correction was applied to the processed spectra in the directly detected ^{1}H dimension. The chemical shifts were referenced to external DSS to ensure consistency among all spectra (*22*).

The backbone amide peaks were picked with FELIX 2000 (Accelrys Inc., San Diego, CA) and compared to previously obtained assignments of Par10 (*23*). Chemical shift differences in the amide proton ($\Delta\delta_{^1HN}$) and nitrogen ($\Delta\delta_{^{15}N}$) resonances of the free and complexed protein forms were combined for each residue by using the expression $[(\Delta\delta_{^1HN})^2 + (\Delta\delta_{^{15}N}/6.5)^2]^{1/2}$ (*24*).

Docking Calculations. The three-dimensional structure model of the complex between Par10 and the peptide **7** core sequence RATFVVDPQGI was calculated with HADDOCK (*25*). Toward this end, CSP data obtained for the Par10−peptide **7** complex were introduced into the structure calculation as ambiguous interaction restraints (AIRs) to drive the docking process. Residues with combined CSP values of > 0.02 ppm were selected as "active AIR restraints" if their relative surface accessibilities were higher than 40%. Surface-accessible residues located next to active AIR residues were selected as "passive AIR restraints". Surface accessibility calculations with NACCESS (*26*) and subsequent docking calculations were conducted using the atomic coordinates of *E. coli* Par10 [Protein Data Bank (PDB) entry 1JNT]. In the calculation procedure, 600 conformers were initially generated using the rigid-body docking protocol. Next, the 50 lowest-energy structures were subjected to semiflexible simulated annealing in torsion angle space, with the side chains of the residues forming the protein−peptide interface left flexible. The resulting top 25 structures were eventually refined in an 8 Å shell of explicit TIP3P (*27*) water molecules.

Construction of a Par10-Negative E. coli Strain. Replacement of the *parA* gene with a chloramphenicol resistance (*cat*) cassette was conducted in *E. coli* strain BT125 (*28*) using the pCVD442 suicide vector (*29*) that encodes β-lactamase for ampicillin resistance and *sacB* from *Bacillus subtilis*. All cloning procedures with this vector were performed in *E. coli* strain SM10αpir (*30*). A 785 bp fragment located upstream and a 933 bp fragment located downstream of the *parA* gene were amplified by PCR using chromosomal DNA of *E. coli* HB101 as a template. Specific oligonucleotide primers were used to insert *Sal*I−*Hin*dIII and *Hin*dIII−*Xba*I restriction sites at the 5′- and 3′-ends of the two DNA fragments, respectively. The identity of the amplified products was determined by DNA sequencing. Fragments were cloned in the pBluescript II KS vector. The resulting 1.7 kb *Sal*I−*Xba*I insert was subcloned in pCVD442. A 3.3 kb *cat* cassette obtained by restriction of vector pRU667 (*31*) was ligated into the *Hin*dIII site between the two cloned DNA fragments mentioned above to yield pCDP1, which contains *cat* resistance surrounded by the upstream and downstream regions of *parA*. For gene replacement, pCDP1 was transformed in competent *E. coli* BT125 cells, which were plated onto LB plates containing 25 μg/mL chloramphenicol to select for crossover events.

Plasmid purification using the rapid alkaline extraction method, production of competent cells, PCR, and cloning procedures were conducted as described previously (*32*). DNA sequencing was performed using the T7 sequencing kit (Pharmacia). Antibiotics and all DNA-modifying enzymes were purchased from Boehringer Mannheim (Mannheim, Germany).

Oxidative Stress Treatment and Disk Inhibition Assay. Oxidative stress to the Par10-negative *E. coli* strain and wild-type BT125 was applied in liquid LB medium. Cells were grown in 5 mL cultures up to an A_{600} of 0.7 and treated for 15 min with 100 μL of H_2O_2 solutions at varying concentrations. After being washed in LB medium, several dilutions of the cultures were spread onto LB plates and incubated overnight at 37 °C. The survival rate after H_2O_2 treatment was determined by counting colony-forming units (CFU) per milliliter of cell culture. For evaluation of each strain and each peroxide concentration, the average number of surviving cells was determined on the basis of five independent experiments.

A disk inhibition assay was used to determine the sensitivity toward H_2O_2 (*33*). An overnight culture (100 μL) grown in M9 minimal medium was added to 2.5 mL of M9 top agar and plated onto M9 plates. Hydrogen peroxide was applied to a 5 mm diameter paper disk placed on the lawn of cells. Plates were incubated at the appropriate temperatures, and after 18 h, the diameters of the killing zones were measured.

RESULTS AND DISCUSSION

E. coli Par10 Interacts with AhpC. The functional relevance of Par10 in the bacterial cell is certainly dependent on its interactions with other cellular components, although no such interaction partners have been identified to date. To this end, *E. coli* cell extracts harboring either recombinant glutathione *S*-transferase (GST) or the GST−Par10 fusion protein were incubated with glutathione Sepharose B for coupling. The recombinant GST−Par10 fusion protein thereby retained full PPIase activity (data not shown) in the protease-coupled PPIase assay (*34*). After elution of bound proteins, analysis by SDS−PAGE indicated the presence of a protein with an apparent molecular mass of ~22 kDa only in the samples derived from the GST−Par10 fusion protein-expressing strain (Figure 1A). Analysis of this 22 kDa band by Edman degradation revealed the SLINTKIKPF sequence as the first 10 N-terminal amino acid residues. Database searches using BlastP identified this sequence as the N-terminus of the peroxiredoxin AhpC from *E. coli* (SwissProt entry P26427). Western blot analyses of the GST−Par10 fusion protein and GST control column eluates with anti-AhpC antiserum revealed that AhpC does bind specifically to GST−Par10 fusion protein-loaded glutathione beads (Figure 1B).

AhpC represents a cysteine-based peroxidase that catalyzes the reduction of hydrogen peroxide, peroxynitrite, and various organic hydroperoxides (*35*). Such antioxidative proteins are known to occur in bacteria, yeast, and mammals for the protection of radical-sensitive cellular components from peroxide-mediated oxidative damage (*36*, *37*). AhpC from *Salmonella typhimurium*, together with a larger FAD-binding subunit (AhpF), reduces peroxides to the corresponding alcohols and water by using NAD(P)H as an electron donor (*38*, *39*). Recent data showed that reduced AhpC exists in vitro as a high-molecular mass oligomer composed of five homodimer subunits that appear like a doughnut-shaped decamer, whereas the oxidized form features

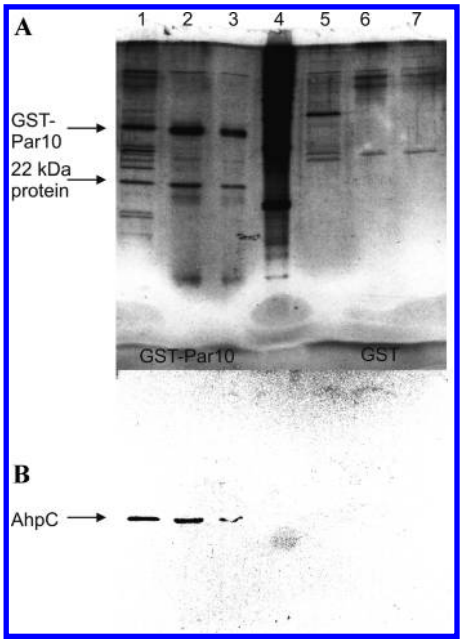

FIGURE 1: GST−Par10 fusion protein specifically interacts with a 22 kDa protein identified as AhpC. (A) Analysis of bound proteins eluted from glutathione Sepharose B coupled with either GST−Par10 fusion protein or GST as a control. Proteins were separated by SDS−PAGE and visualized by silver staining: lanes 1−3, 15 μL fractions eluted from the GST−Par10 fusion protein-coupled column; lane 4, molecular mass marker; lanes 5−7, 15 μL fractions eluted from the GST-coupled column. (B) Identification of the 22 kDa protein as AhpC by Western blot analysis using anti-AhpC antiserum. The lanes are the same as those of panel A.

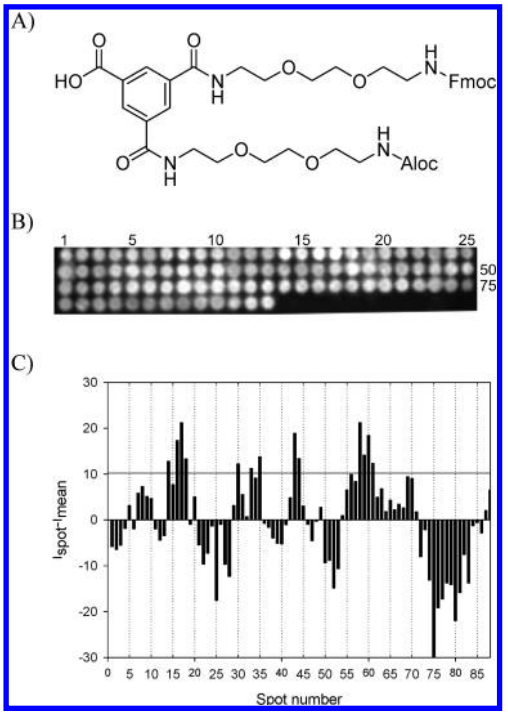

FIGURE 2: (A) Structural formula of the orthogonally protected trimesic acid derivative linker **1**. (B) The fluorescence of the cellulose membrane was recorded after irradiation with UV light at 312 nm and subsequent selection with a "Sybr green" filter. (C) Densitometric analysis of panel B. The top control line represents the standard deviation from average fluorescence intensity. A positive value above the top control line on this arbitrary unit scale indicates a potential interaction of the peptides in a particular pair. At least two consecutive spots with fluorescence intensity higher than the standard deviation were indicative of a nativelike interaction.

dimers or decamers depending on the concentration (*35*, *40*). Several studies have suggested an exchange between the AhpC decamer and dimer states during the catalytic cycle, with the decameric form featuring increased peroxidase activity (*41*, *42*). The physiological role of this dimer−decamer transition, however, is still not fully understood. Using cross-linking experiments, we found that Par10 interacts mostly with monomeric AhpC, while only minor cross-link products of Par10 with the AhpC dimer and AhpF monomer were detected (Figure S1 of the Supporting Information).

Screening for Protein−Protein Binding Sites Using the IANUS Peptide Array. Because of its pronounced oligomerization propensity, AhpC (*35*) presumably would not present the entire set of potential interaction interfaces in a conventional array of Par10-derived peptides. Thus, to reveal the contact regions of both interaction partners, the IANUS peptide array was applied. Thereby, protein−protein interactions are represented by and investigated as template-assisted peptide−peptide interactions using fluorescein- and dansyl-labeled peptide pairs that are immobilized on a solid support. The IANUS peptide array has at least two advantages over standard microarrays using spot synthesis: (i) the binding regions of both proteins can be analyzed in just one experiment, and (ii) the physical presence of natively folded soluble proteins or antibodies is not required.

A major issue with regard to the IANUS peptide array is its performance in the identification of template-assisted intramolecular interactions of peptide pairs. Fluorescence resonance energy transfer (FRET) is a well-known method for measuring inter- and intramolecular distances in biomolecular studies (*43*, *44*). In this work, FRET was used to differentiate between interacting and noninteracting peptide pairs in the IANUS peptide array.

To screen all possible peptide combinations of both proteins, i.e., overlapping 12-mer peptides that fully scan through each protein sequence with a frame shift of two amino acids, a library of 3696 peptide pairs would have been needed. Because of the known three-dimensional structure of Par10 in solution (*23*) and the structural similarity between Par10 and the PPIase domain of human Pin1, residues L49, M57, and F61 were assigned to take part in the formation of the substrate-binding site of Par10, while residues H8, C40, F81, and H84 were thought to be directly involved in catalysis (*23*). To support the hypothesis that Par10 interacts with AhpC via its PPIase site, we screened AhpC peptides encompassing the full-length protein with the active site-derived L49−F61 sequence of Par10, thus drastically reducing the size of the peptide library.

At first, the orthogonally protected trifunctional linker **1** (Figure 2A) was attached to the derivatized cellulose membrane. Next, using a standard spot technique (*21*), 88 overlapping 12-mer peptides spanning the entire AhpC sequence were synthesized on the Fmoc site of linker **1**. A β-Ala residue was coupled to the N-terminus of each peptide followed by 5(6)-carboxyfluorescein. After cleavage of the Aloc protective group, the sequence of the Par10 substrate-binding site (i.e., LGEFRQGQMVPAF) was synthesized as a second peptide chain in all spots and subsequently labeled with dansyl chloride. After cleavage of all side chain protecting groups, interacting peptide pairs were detected by irradiating the membrane with UV light at 312 nm; the resulting fluorescence emission was filtered at 520 nm and recorded (Figure 2B).

Table 1: Synthesized Peptides

peptide	sequence	spot numbers
2	Ac-SLINTKIKPFKNQAFK-NH_2	1−3
3	Ac-QAFKNGEFIEITEKDTEG-NH_2	7−10
4	Ac-RWSVFFFYPADFTFV-NH_2[a]	16−18
5	Ac-VDVYAVSTDTHFTHKA-NH_2	33−35
6	Ac-SETIAKIKYAMIGD-NH_2	43 and 44
7	Ac-GLADRATFVVDPQGIIQA-NH_2	58−61
8	Ac-SHPGEVCPAKWK-NH_2	80
9	Ac-EATLAPSLDLVGKI-NH_2	87 and 88

[a]Peptide **4** was synthesized without a Cys residue at the C-terminus, although this residue was present at the C-terminus of the peptide in spot 18.

As expected, the resulting microarray image presented different fluorescence values for the microarray spots (Figure 2B). Given the inhomogeneities of the cellulose matrix and the lack of a suitable internal standard for distance calculations in the IANUS peptide spot array, a comparison of relative spot fluorescence intensities was used to identify interacting peptide pairs. They are expected to exhibit a stronger FRET effect due to interaction-induced chain proximity, resulting in higher spot fluorescence intensities. Two or more consecutive spots with fluorescence intensity higher than the standard deviation from average fluorescence intensities were termed IANUS-positive spots and considered indicative of a nativelike interaction. Several such spot regions with a strong fluorescence signal were thus detected by densitometric analysis (Figure 2C), revealing peptides **4**, **6**, and **7** (Table 1) as potential ligands for the Par10 substrate-binding site. This was confirmed by their subsequent emergence as the most potent Par10 inhibitors in the PPIase assay described below. Certainly, the possibility that additional interaction sites exist between AhpC and Par10 cannot be ruled out, but these most likely would not be relevant to Par10 enzymatic activity.

According to the crystal structure, AhpC from *S. typhimurium* (a 20.6 kDa protein that differs in only three residues from *E. coli* AhpC) forms a stable oligomeric complex of 10 subunits in the reduced state (*40*). Peptide **4**, which represents the AhpC segment of residues R31−V45 and interacts most strongly with Par10, is part of this AhpC oligomerization interface. The second IANUS-positive hit, namely peptide **6**, corresponds to AhpC residues S85−D98 that comprise β-strand 5 as well as the 3_{10}-helix region, identified as the main difference in the sequences of the eukaryotic peroxide-sensitive 2-Cys peroxiredoxins compared to the more robust bacterial counterparts. Peptide **7**, finally, representing the AhpC segment G115−A132, includes β-strands 6 and 7 as well as the surface-exposed turn of residues D125−I129 between them, which features residue P126 as a potential Par10 target.

Inhibition of Par10 Catalytic Activity by the Interacting Peptides. Peptides **4**, **6**, and **7** (Table 1) were tested in the protease-free PPIase assay for their ability to inhibit Par10 catalytic activity. Measurements of Par10 PPIase activities were based on isomer-specific intramolecular fluorescence quenching (*45*, *46*), using the Abz-Ala-Leu-Pro-Phe-pNa peptide as substrate. Aminobenzoyl (Abz) fluorescence is suppressed much more strongly by the *p*-nitroanilide (pNa) quencher when the peptidyl prolyl bond of the substrate is in the *cis* conformation (*47*). The time-dependent *cis*−*trans* isomerization of the Leu−Pro bond after a solvent jump from a LiCl/TFE solution into HEPES buffer can be monitored by fluorescence enhancement. The rate constant of *cis*−*trans* isomerization ($k_{c/t}$) depends on the Par10 concentration (Figure 3A,B) and the inhibitory potential of the investigated peptide (Figure 3C,D).

The protease-free PPIase assay was performed with peptides **2**−**9**, of which the following peptides were considered as negative controls: (i) peptides **2** and **8** from spot regions with lower than average florescence intensities (i.e., negative values in Figure 2C) and (ii) peptides **3**, **5**, and **9** from spot regions with stronger than average fluorescence intensities that nevertheless did not yet fulfill the predefined conditions for nativelike interactions. All of these negative controls showed no significant inhibition of Par10 PPIase activity, while the IANUS-positive hits, i.e., peptides **4**, **6**, and **7**, emerged also in the protease-free PPIase assay as the most potent interaction partners for the Par10 substrate-binding site. Peptides **4** and **7**, which both contain a single Pro residue and are thus biologically relevant, inhibit Par10 catalytic activity with IC_{50} values of 34.3 and 62.1 μM, respectively.

Localization of the Par10 Peptide-Binding Region by NMR. To pinpoint the interaction sites between Par10 and its potential ligands, chemical shift perturbation (CSP) experiments, which are capable of detecting even transient binding interactions in the lower micromolar affinity range, were performed. When the peptide binds to ^{15}N-labeled Par10, changes in the chemical shift values of nearby backbone amide groups were expected to occur in ^{1}H−^{15}N HSQC spectra. The resulting CSP effects were analyzed on the basis of previously reported ^{1}H and ^{15}N resonance assignments of Par10 (*23*).

Because of its very low solubility in aqueous buffer, peptide **4** could not be used for the NMR experiments. Instead, we investigated peptide **7** (Figure S2 of the Supporting Information), as the second-best Par10 inhibitor, and His_6-AhpC (in its reduced oligomeric form) to determine the interaction site of Par10. CSP effects observed in NMR spectra of ^{15}N-labeled Par10 upon addition of each interaction partner (Figure 4) indicated the same general contact region, which furthermore coincides with the previously proposed substrate-binding pocket.

Interaction of Par10 with peptide **7** produced considerable combined ^{1}H and ^{15}N chemical shift changes ($\geq$0.015 ppm) of the amide proton resonances belonging to residues S42, L49, G50, R53, Q54, M57, V58, A60, F61, K63, and F81 (Figure 4A), most of which are located at the proposed substrate-binding site defined by L49, M57, and F61 (*23*). Among the residues whose amide protons exhibited weaker but still notable shifts were H8, C40, and H84, which (together with F81) have been associated with the Par10 catalytic cascade (*23*).

In the case of the Par10−His_6-AhpC complex, smaller shift differences were observed (Figure 4B) compared to those of the peptide **7** complex, but once again involving residues M57 and V58 at the proposed substrate-binding site. Although the CSP effects upon binding of full-length AhpC appear to be weaker than in the case of the peptide, the line broadening observed in the ^{1}H−^{15}N HSQC spectra of ^{15}N-labeled Par10 with increasing His_6-AhpC concentrations (Figure S3 of the Supporting Information) provides additional evidence for the formation of a high-molecular mass protein−protein complex. As reduced His_6-AhpC exists in the NMR sample primarily in decameric form (deduced from the line width in one-dimensional ^{1}H NMR spectra), Par10 has to compete with other AhpC molecules for binding to a single AhpC moiety. Hence, it appears that the observed contacts on the Par10 surface derive from small amounts of either monomeric AhpC or other AhpC forms present under these conditions. This circumstance would furthermore explain

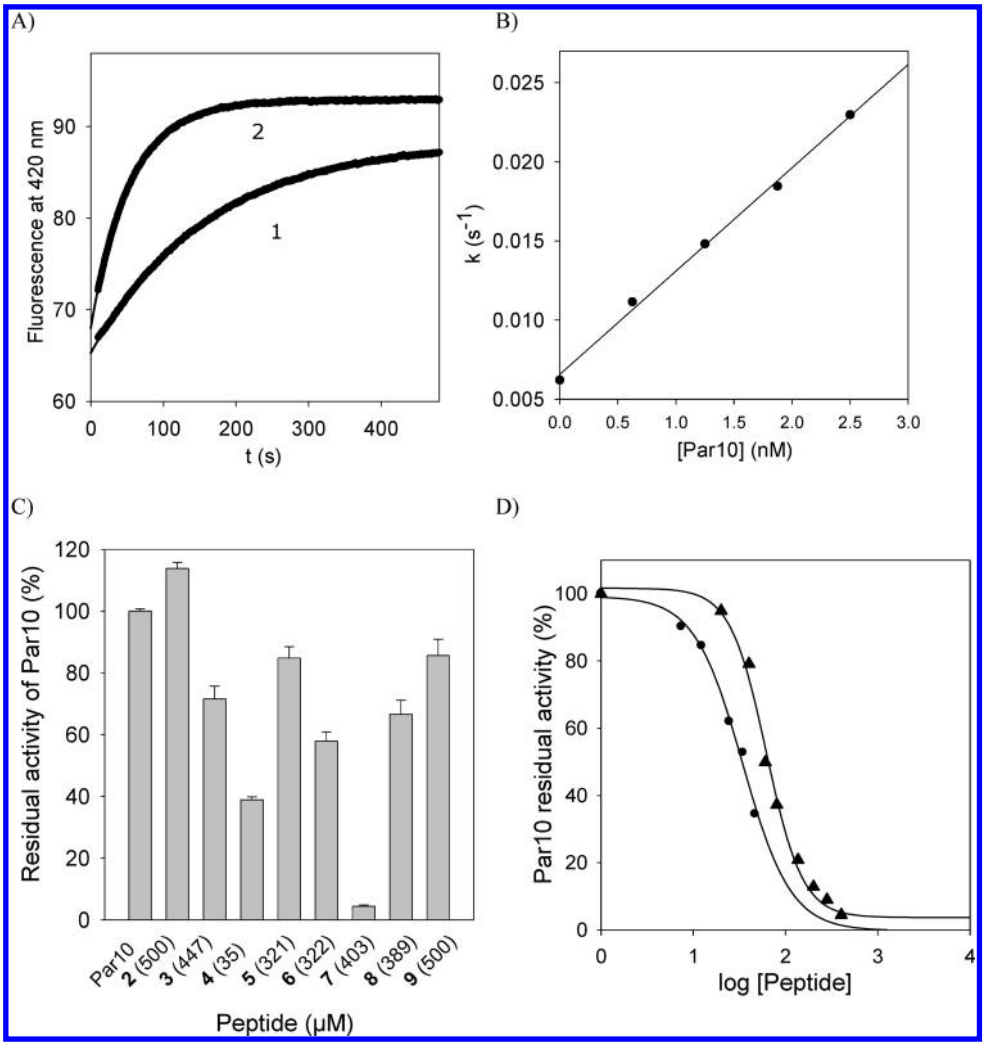

FIGURE 3: (A) Kinetics of *cis*−*trans* imide bond isomerization of the substrate Abz-Ala-Leu-Pro-Phe-pNa following a solvent jump from a LiCl/TFE solution into HEPES buffer (pH 7.8) at 10 °C (1) in the absence of Par10 or (2) with 1.9 nM Par10. (B) Dependence of the first-order rate constant $k_{c/t}$ on Par10 concentration. (C) Inhibition of Par10 (1.9 nM) catalytic activity by peptides **2**−**9**. (D) Determination of IC_{50} values for peptides **4** [IC_{50} = 34.3 μM (●)] and **7** [IC_{50} = 62.14 μM (▲)]. A sigmoidal dose−response curve fit with a variable slope of approximately −2 was used.

why neither the enzymatic activity of AhpC in a peroxidase assay (*38*, *48*) nor the PPIase activity of Par10 was influenced significantly by the interaction between both proteins (data not shown).

To assess whether peptide **7** is merely a Par10 inhibitor or actually a competitive substrate in the enzyme assay, i.e., whether the *cis*−*trans* isomerization of the prolyl imide bond is accelerated by Par10, 2D NOESY spectra of peptide **7** were recorded both in the absence and in the presence of a catalytic amount of Par10, in analogy to a previously described procedure (*49*). Remarkably, upon addition of Par10 to peptide **7**, exchange peaks between the Pro Hδ resonances of peptide **7** in the *trans* (3.86 and 3.82 ppm) and *cis* (3.56 and 3.50 ppm) configuration emerged (Figure 5). This result demonstrates that Par10 catalyzes the *cis*−*trans* isomerization of the Asp−Pro imide bond of peptide **7**, thus corroborating the fact that peptide **7**, which was originally identified by the IANUS peptide array as a potential Par10 ligand, can be in fact considered a Par10 substrate.

Structural Insights into the Complex between Par10 and Peptide 7. To obtain a model for the binding interaction of Par10 with peptide **7**, we performed docking calculations on the basis of the CSP data. The most strongly affected Par10 residues (S42, G50, R53, M57, and F81) were selected as active AIRs, whereas V58 and A60 were excluded because of their low (< 40%) surface accessibilities. The following residues that (i) are adjacent to active AIR residues and (ii) display a surface accessibility of > 40% were additionally selected as passive AIRs: L10, K12, P41, K44, R45, D48, E51, Q54, G55, Q56, and Q80. The locations of the active and passive AIRs that comprise the interaction region of the protein are shown in Figure 6A.

As preliminary docking trials with the full peptide **7** sequence were inconclusive, we decided to truncate the ligand in silico. The consensus sequence of IANUS peptide spots 58−61, i.e., peptide **7** residues TFVVDPQ, were all selected as active AIRs. In addition, two residues each were kept at the N- and C-terminal ends, with the ones right next to the active AIR sequence designated as passive AIRs. This proline-containing core segment RATFVVDPQGI, corresponding to AhpC residues R119−I129, was henceforth used for further docking calculations.

Interestingly, the best docking result was obtained when the Pro residue of the peptide was kept in the *cis* configuration, despite the fact that both in the AhpC crystal structure and in the peptide **7** solution conformation the *trans* configuration is predominant in this prolyl peptide bond (Figure S4 of the Supporting Information). The 20 energetically most favorable

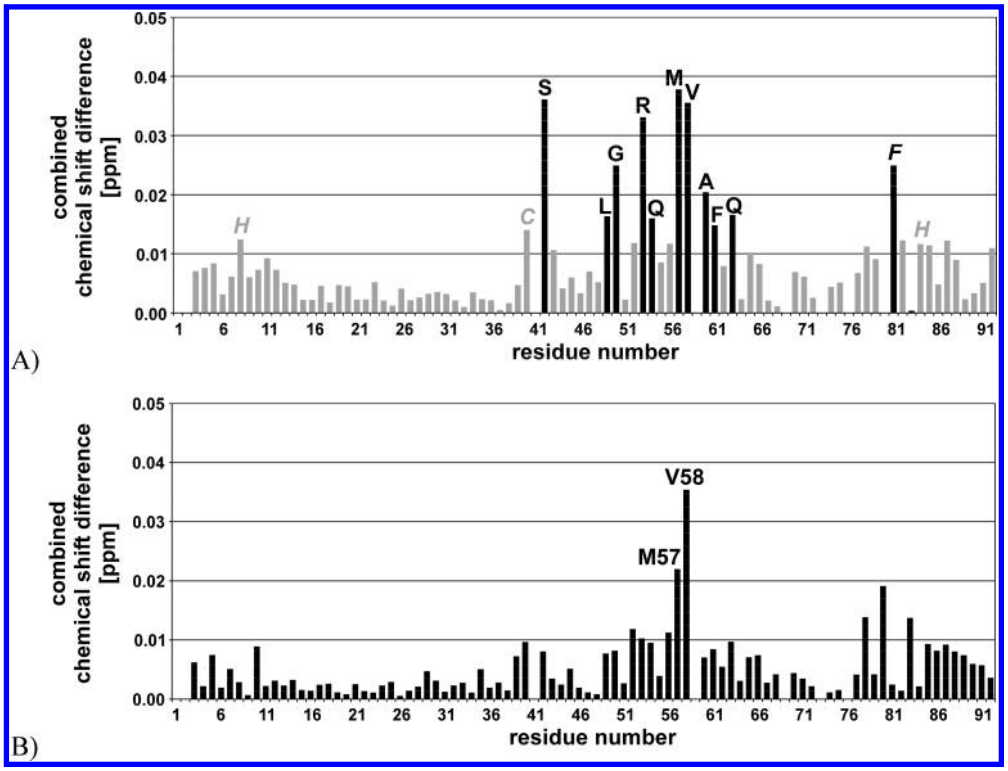

FIGURE 4: Combined ^{1}H and ^{15}N chemical shift perturbation data of the *E. coli* Par10 backbone amide groups in the presence of (A) peptide **7** and (B) full-length AhpC. In panel A, residues showing a combined chemical shift difference of ≥0.015 ppm are indicated by black bars and labels in one-letter code; residues associated with the catalytic cascade (i.e., H8, C40, F81, and H84) are additionally indicated in italics. In panel B, the most prominent CSP effects were observed for residues M57 and V58 in the proposed substrate-binding site.

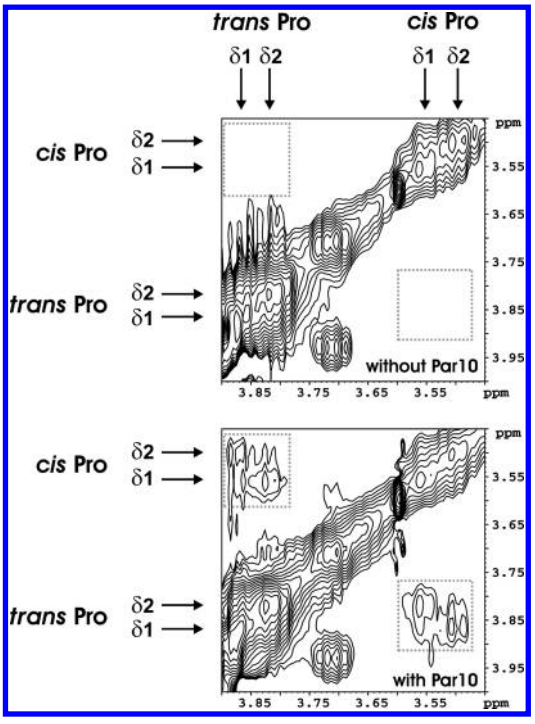

FIGURE 5: Sections from the homonuclear 2D NOESY spectra of peptide **7** (3 mM) recorded for 3 days at 25 °C in the absence (top) and presence (bottom) of nonlabeled *E. coli* Par10 (22 μM). Arrows indicate the positions of the Pro Hδ resonances of peptide **7** when the proline residue is in the *trans* (3.86 and 3.82 ppm) or *cis* (3.56 and 3.50 ppm) configuration. Gray dotted boxes mark the positions where exchange signals between the Hδ resonances of the two different Pro isomers are expected to occur. The level of chemical exchange due to proline peptide bond isomerization is increased considerably in the presence of the PPIase Par10.

conformers displayed a strong structural consensus, with the Asp side chain of peptide **7** buried in the substrate-binding pocket of Par10 between H8 and H84, while the Pro ring is sandwiched between C40 and F81 (Figure 6B). Moreover, the first Val residue forms hydrophobic contacts with Par10 residues L49 and M57.

This structural arrangement is in good agreement with the CSP data described above, because the most strongly affected Par10 surface residues define the contact site, with the exception of residues V58 and A60, whose low surface accessibilities (ca. 10%) suggest that their perturbation upon ligand binding may be attributed to secondary effects (i.e., changes in conformation or electronic shielding beyond the contact interface). Moreover, the resulting complex structure corroborates the fact that the strong fluorescence observed in IANUS peptide spots 58−61 is the result of interactions between the AhpC-derived peptides and the Par10 sequence of residues L49−F61, which was used as second peptide chain in the IANUS peptide array.

The docking calculations revealed a model of the Par10−peptide complex in which the residues corresponding to the AhpC segment R119−Q127 show direct surface contacts with Par10 (with the side chains of V123, D125, and Pro126 fully immersed), amounting to a total buried surface area of 1308 Å^2. Interestingly, both the Pro and the preceding Asp residue of the peptidic substrate show direct contacts with the four Par10 residues that have been associated with the proposed catalytic cascade: the Pro residue (in the *cis* conformation, as expected for a Par10 substrate) is located between Par10 residues C40 and F81, while the side chain of the Asp residue features hydrogen bond contacts with H8 and H84 (Figure 6B). It could be envisioned that the hydrophobic phenyl ring of F81 attracts the peptidic Pro residue to this particular position, as is the case also in the substrate complex of the

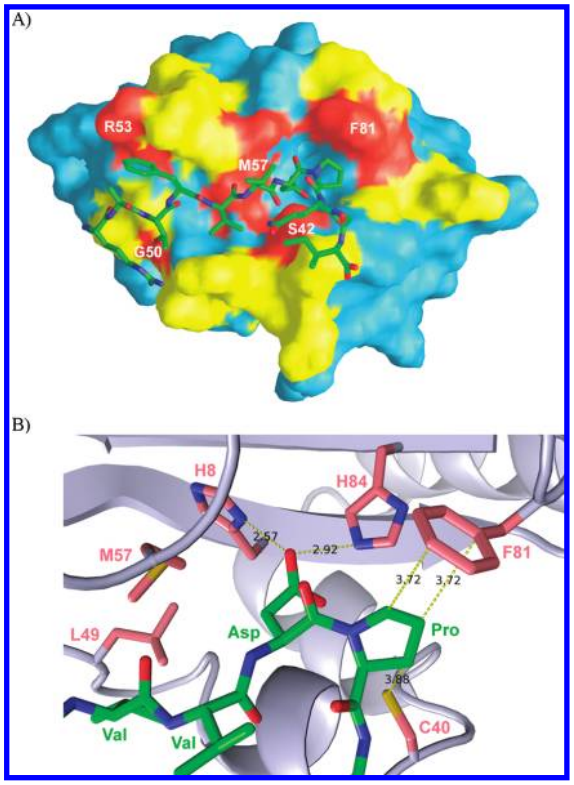

FIGURE 6: Docking model of the Par10−peptide **7** complex. (A) Graphic representation of the complex between Par10 (surface) and the peptide (rods). Active and passive AIR residues of Par10 are colored orange (with labels) and yellow, respectively. (B) Close-up of the substrate-binding site, showing the intermolecular side chain contacts between Par10 (light red labels) and the peptide (green labels).

analogous human Pin1 (*50*). Moreover, the interaction of the Asp carboxylate group with both imidazole rings inside the protein cavity could additionally fixate the substrate to Par10 and possibly affect the proton transfer in the catalytic cascade, which was recently proposed for the parvulin-type PPIase from *Staphylococcus aureus*, while a similar role for the corresponding histidine residues in human Pin1 was ruled out by another group (*51*, *52*). At this point, the structural arrangement of this Par10−substrate complex certainly does not explain how the catalysis proceeds, but it might provide fundamental information that could become helpful in the future in the elucidation of the catalytic mechanism of Par10 and related PPIases.

Increased Sensitivity of the Par10-Negative E. coli Strain to Oxidative Stress. To investigate the involvement of *E. coli* Par10 in the cellular oxidative stress response, we replaced chromosomally encoded *parA* with a *cat* cassette encoding resistance toward chloramphenicol. A combined genetic−physical map of the 10−15 kb segment from the region between 84.5 and 86.5 min on the *E. coli* genome was deduced from the physical map (*53*). The correct chromosomal organization of the exchanged region in the Par10-negative *E. coli* strain was checked by Southern blot analysis (data not shown). The lack of Par10 was confirmed by immunoprecipitations of cell extracts from *E. coli* BT125 and the Par10-negative *E. coli* strain using anti-Par10 antiserum followed by Western blot analysis (Figure S5 of the Supporting Information).

The treatment of the Par10-negative *E. coli* strain with hydrogen peroxide revealed a special phenotype that exhibited increased sensitivity toward oxidative stress. Especially at higher concentrations of the peroxide, the viability of the mutant strain

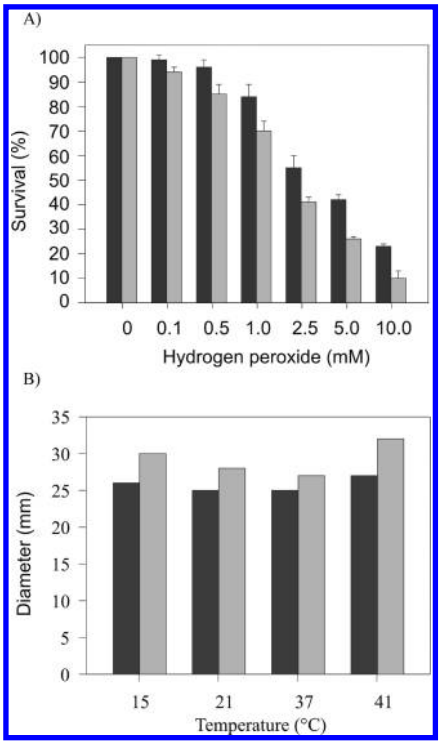

FIGURE 7: (A) Effect of hydrogen peroxide treatment on the Par10-negative *E. coli* strain in comparison to its wild type. Wild-type cells (black bars) and the Par10-negative strain (gray bars) were grown in Luria broth up to an A_{600} of 0.7. The strains were treated with the indicated concentrations of hydrogen peroxide, washed, and plated in several dilutions on selective medium. The rate of survival was evaluated by CFU count after overnight incubation. (B) Disk inhibition assay of BT125 (wild type) and the Par10-negative strain. Cultures of BT125 (black bars) and Par10-negative (gray bars) *E. coli* strains were plated onto minimal plates, and H_2O_2 was applied on a paper disk in the middle of the plate. The killing zones were measured after overnight incubation at the indicated temperatures.

in the exponential growth phase was decreased compared to that of wild-type *E. coli* (Figure 7A).

This phenotype of the Par10-negative *E. coli* mutant was confirmed by disk inhibition assays with hydrogen peroxide. When mutant cells were cultivated at nonoptimal temperatures (≠37 °C), an increased sensitivity toward peroxide as a stress factor was observed, as reflected by increased killing zone diameters in disk inhibition assays (Figure 7B). In the absence of the stress factor, the Par10-negative *E. coli* strain and wild-type BT125 did not exhibit any differences in growth rates (data not shown).

According to the thioredoxin peroxidase pathway (*54*), the Cys46 SH group of AhpC is selectively oxidized by peroxide to a Cys46 SOH group at the beginning of the catalytic process. The Cys46 SOH group then reacts with the Cys165 SH group of the other AhpC subunit to form an intermolecular disulfide bond. The disulfide bond is considered to be resistant to further oxidation (*55*), although it was shown recently that disulfide bonds, at least in cyclic peptides, can be easily oxidized further (*56*). At the end of the catalytic cycle, the disulfide bond is reduced by AhpF using 1 equiv of NADPH. For the formation of the disulfide bond, a conformational rearrangement from fully folded to locally unfolded AhpC is required. The rate of this conformational change is directly involved in irreversible AhpC inactivation by overoxidation. It should be pointed out that the sequence of residues R31−V45 of AhpC, i.e., peptide **4** found by the IANUS peptide array as a Par10 interaction partner, is located next to the oxidation-sensitive Cys46 residue. Thus, it

would not be surprising if a folding-helper enzyme such as Par10, aside from expediting the correct folding of AhpC produced de novo under stress conditions, could also enhance the equilibrium rate of unfolding needed for disulfide bond formation, thereby (i) protecting AhpC against overoxidation and (ii) improving the rate of the entire catalytic cycle. In fact, our search for a particular characteristic of the Par10-negative *E. coli* strain revealed a phenotype with decreased survival rates compared to that of the wild type upon treatment with hydrogen peroxide. This effect was stronger at high peroxide concentrations, when the rate of the catalytic cycle became more important, and could be additionally enhanced by temperature stress.

Previously, deletions of either AhpC or AhpF as well as chromosomal mutations in the respective genes (*ahpC* and/or *ahpF*) all resulted in hypersensitivity toward several organic peroxides both in *E. coli* and in *S. typhimurium* (*57*, *58*). As expected for a folding-helper enzyme, the hypersensitivity observed upon Par10 deletion in *E. coli* is less striking. Presumably, other immunophilins in the bacterial cell (*59*, *60*) compensate for the lack of Par10.

CONCLUSIONS

In summary, these studies have unequivocally demonstrated that the IANUS peptide array, when probed by FRET detection, has identified the physiologically relevant interaction interfaces of the peroxiredoxin AhpC with the parvulin-type *E. coli* PPIase Par10. Furthermore, final proof for the location of the Par10 substrate-binding pocket was obtained from NMR-based CSP experiments and docking calculations. Our results thus provide support for an AhpC−Par10 binding interaction that implicates a catalyzed prolyl *cis*−*trans* isomerization of AhpC during the oxidative stress response of *E. coli*.

ACKNOWLEDGMENT

We are grateful to A. Schierhorn for performing mass spectrometry, P. Rücknagel for the Edman degradation experiment, and C. Gershing, I. Kunze, K. Jentzsch, and M. Seidel for technical assistance.

SUPPORTING INFORMATION AVAILABLE

Analysis of the interaction among Par10, His_6-AhpC, and His_6-AhpF by chemical cross-linking; overlay of two $^1H-^{15}N$ HSQC spectra recorded with ^{15}N-labeled *E. coli* Par10 in the absence and presence of peptide **7**; one-dimensional traces through the V58 signal in the ^1H dimension of the $^1H-^{15}N$ HSQC spectra; immunoprecipitation and Western blot analysis of Par10-negative and BT125 wild-type *E. coli* strains; peptides synthesized in each spot of the cellulose membrane; cloning, overexpression, and characterization of recombinant *E. coli*-derived AhpC and AhpF; cloning and overexpression of recombinant *E. coli* Par10; and peptide synthesis, HPLC, protein sequencing, peptide mapping, and mass spectroscopy. This material is available free of charge via the Internet at http://pubs.acs.org.

REFERENCES

1. Frank, R. (2002) The SPOT-synthesis technique. Synthetic peptide arrays on membrane supports—principles and applications. *J. Immunol. Methods 267*, 13–26.
2. Wenschuh, H., Volkmer-Engert, R., Schmidt, M., Schulz, M., Schneider-Mergener, J., and Reineke, U. (2000) Coherent membrane supports for parallel microsynthesis and screening of bioactive peptides. *Biopolymers 55*, 188–206.
3. Reimer, U., Reineke, U., and Schneider-Mergener, J. (2002) Peptide arrays: From macro to micro. *Curr. Opin. Biotechnol. 13*, 315–320.
4. Volkmer, R. (2009) Synthesis and application of peptide arrays: Quo vadis SPOT technology. *ChemBioChem 10*, 1431–1442.
5. Yu, C., Malesevic, M., Jahreis, G., Schutkowski, M., Fischer, G., and Schiene-Fischer, C. (2005) The architecture of protein-ligand binding sites revealed through template-assisted intramolecular peptide-peptide interactions. *Angew. Chem., Int. Ed. 44*, 1408–1412.
6. Fanghänel, J., and Fischer, G. (2004) Insights into the catalytic mechanism of peptidyl prolyl *cis*/*trans* isomerases. *Front. Biosci. 9*, 3453–3478.
7. Lu, K. P., Finn, G., Lee, T. H., and Nicholson, L. K. (2007) Prolyl *cis*-*trans* isomerization as a molecular timer. *Nat. Chem. Biol. 3*, 619–629.
8. Wedemeyer, W. J., Welker, E., and Scheraga, H. A. (2002) Proline *cis*-*trans* isomerization and protein folding. *Biochemistry 41*, 14637–14644.
9. Fischer, G., and Aumüller, T. (2003) Regulation of peptide bond *cis*/*trans* isomerization by enzyme catalysis and its implication in physiological processes. *Rev. Physiol. Biochem. Pharmacol. 148*, 105–150.
10. Luan, S., Albers, M. W., and Schreiber, S. L. (1994) Light-regulated, tissue-specific immunophilins in a higher plant. *Proc. Natl. Acad. Sci. U.S.A. 91*, 984–988.
11. Dolinski, K., Muir, S., Cardenas, M., and Heitman, J. (1997) All cyclophilins and FK506 binding proteins are, individually and collectively, dispensable for viability in *Saccharomyces cerevisiae*. *Proc. Natl. Acad. Sci. U.S.A. 94*, 13093–13098.
12. Missiakas, D., Betton, J. M., and Raina, S. (1996) New components of protein folding in extracytoplasmic compartments of *Escherichia coli* SurA, FkpA and Skp/OmpH. *Mol. Microbiol. 21*, 871–884.
13. Dartigalongue, C., and Raina, S. (1998) A new heat-shock gene, ppiD, encodes a peptidyl-prolyl isomerase required for folding of outer membrane proteins in *Escherichia coli*. *EMBO J. 17*, 3968–3980.
14. Lee, J. P., Palfrey, H. C., Bindokas, V. P., Ghadge, G. D., Ma, L., Miller, R. J., and Roos, R. P. (1999) The role of immunophilins in mutant superoxide dismutase-1 linked familial amyotrophic lateral sclerosis. *Proc. Natl. Acad. Sci. U.S.A. 96*, 3251–3256.
15. Doyle, V., Virji, S., and Crompton, M. (1999) Evidence that cyclophilin-A protects cells against oxidative stress. *Biochem. J. 341*, 127–132.
16. Wen, Z. T., Suntharaligham, P., Cvitkovitch, D. G., and Burne, R. A. (2005) Trigger factor in *Streptococcus mutans* is involved in stress tolerance, competence development, and biofilm formation. *Infect. Immun. 73*, 219–225.
17. Rahfeld, J. U., Schierhorn, A., Mann, K., and Fischer, G. (1994) A novel peptidyl-prolyl *cis*/*trans* isomerase from *Escherichia coli*. *FEBS Lett. 343*, 65–69.
18. Rahfeld, J. U., Rücknagel, K. P., Schelbert, B., Ludwig, B., Hacker, J., Mann, K., and Fischer, G. (1994) Confirmation of the existence of a third family among peptidyl-prolyl *cis*/*trans* isomerases. Amino acid sequence and recombinant production of parvulins. *FEBS Lett. 352*, 180–184.
19. Hennig, L., Christner, C., Kipping, M., Schelbert, B., Rücknagel, K. P., Grabley, S., Küllertz, G., and Fischer, G. (1998) Selective inactivation of parvulin-like peptidyl-prolyl *cis*/*trans* isomerases by juglone. *Biochemistry 37*, 5953–5960.
20. Malesevic, M., Lücke, C., and Jahreis, G. (2005) Simple and efficient synthesis of new trifunctional templates. In Peptides 2004, Proceedings of the Third International and Twenty-Eighth European Peptide Symposium, pp 391−392, Kenes International, Ben-Gurion, Israel.
21. Frank, R. (1992) Spot-Synthesis: An Easy Technique for the Positionally Addressable, Parallel Chemical Synthesis on a Membrane Support. *Tetrahedron 48*, 9217–9232.
22. Wishart, D. S., Bigam, C. G., Yao, J., Abildgaard, F., Dyson, H. J., Oldfield, E., Markley, J. L., and Sykes, B. D. (1995) ^1H, ^{13}C and ^{15}N chemical shift referencing in biomolecular NMR. *J. Biomol. NMR 6*, 135–140.
23. Kühlewein, A., Voll, G., Hernandez Alvarez, B., Kessler, H., Fischer, G., Rahfeld, J. U., and Gemmecker, G. (2004) Solution structure of *Escherichia coli* Par10: The prototypic member of the Parvulin family of peptidyl-prolyl *cis*/*trans* isomerases. *Protein Sci. 13*, 2378–2387.
24. Mulder, F. A. A., Schipper, D., Bott, R., and Boelens, R. (1999) Altered flexibility in the substrate-binding site of related native and engineered high-alkaline *Bacillus* subtilisins. *J. Mol. Biol. 292*, 111–123.
25. Dominguez, C., Boelens, R., and Bonvin, A. M. J. J. (2003) HADDOCK: A protein-protein docking approach based on biochemical or biophysical information. *J. Am. Chem. Soc. 125*, 1731–1737.
26. Hubbard, S. J., and Thornton, J. M. (1993) NACCESS Computer Program, Department of Biochemistry and Molecular Biology, University College London, London.

27. Jorgensen, W. L., Chandrasekhar, J., Madura, J. D., Impey, R. W., and Klein, M. L. (1983) Comparison of simple potential functions for simulating liquid water. *J. Chem. Phys. 79*, 926–935.
28. Cherepanov, P. P., and Wackernagel, W. (1995) Gene disruption in *Escherichia coli*: TcR and KmR cassettes with the option of Flp-catalyzed excision of the antibiotic-resistance determinant. *Gene 158*, 9–14.
29. Donnenberg, M. S., and Kaper, J. B. (1991) Construction of an eae deletion mutant of enteropathogenic *Escherichia coli* by using a positive-selection suicide vector. *Infect. Immun. 59*, 4310–4317.
30. Simon, R., Priefer, U., and Pühler, A. (1983) A broad host range mobilization system for *in vivo* genetic engineering: Transposon mutagenesis in Gram-negative bacteria. *Nat. Biotechnol. 1*, 784–791.
31. Ubben, D., and Schmitt, R. (1986) Tn1721 derivatives for transposon mutagenesis, restriction mapping and nucleotide sequence analysis. *Gene 41*, 145–152.
32. Sambrook, J., Fritsch, E. F., and Maniatis, T. (1989) Molecular Cloning: A Laboratory Manual, Cold Spring Harbor Laboratory Press, Plainview, NY.
33. Christman, M. F., Morgan, R. W., Jacobson, F. S., and Ames, B. N. (1985) Positive control of a regulon for defenses against oxidative stress and some heat-shock proteins in *Salmonella typhimurium*. *Cell 41*, 753–762.
34. Fischer, G., Wittmann-Liebold, B., Lang, K., Kiefhaber, T., and Schmid, F. X. (1989) Cyclophilin and peptidyl-prolyl *cis-trans* isomerase are probably identical proteins. *Nature 337*, 476–478.
35. Poole, L. B. (2005) Bacterial defenses against oxidants: Mechanistic features of cysteine-based peroxidases and their flavoprotein reductases. *Arch. Biochem. Biophys. 433*, 240–254.
36. Chae, H. Z., Uhm, T. B., and Rhee, S. G. (1994) Dimerization of thiol-specific antioxidant and the essential role of cysteine 47. *Proc. Natl. Acad. Sci. U.S.A. 91*, 7022–7026.
37. Spector, A. (1995) Oxidative stress-induced cataract: Mechanism of action. *FASEB J. 9*, 1173–1182.
38. Jacobson, F. S., Morgan, R. W., Christman, M. F., and Ames, B. N. (1989) An alkyl hydroperoxide reductase from *Salmonella typhimurium* involved in the defense of DNA against oxidative damage. Purification and properties. *J. Biol. Chem. 264*, 1488–1496.
39. Poole, L. B., Godzik, A., Nayeem, A., and Schmitt, J. D. (2000) AhpF can be dissected into two functional units: Tandem repeats of two thioredoxin-like folds in the N-terminus mediate electron transfer from the thioredoxin reductase-like C-terminus to AhpC. *Biochemistry 39*, 6602–6615.
40. Wood, Z. A., Poole, L. B., Hantgan, R. R., and Karplus, P. A. (2002) Dimers to doughnuts: Redox-sensitive oligomerization of 2-cysteine peroxiredoxins. *Biochemistry 41*, 5493–5504.
41. Barranco-Medina, S., Lázaro, J. J., and Dietz, K. J. (2009) The oligomeric conformation of peroxiredoxins links redox state to function. *FEBS Lett. 583*, 1809–1816.
42. Hall, A., Karplus, P. A., and Poole, L. B. (2009) Typical 2-Cys peroxiredoxins: Structures, mechanisms and functions. *FEBS J. 276*, 2469–2477.
43. Wu, P., and Brand, L. (1994) Resonance energy transfer: Methods and applications. *Anal. Biochem. 218*, 1–13.
44. Sapsford, K. E., Berti, L., and Medintz, I. L. (2006) Materials for fluorescence resonance energy transfer analysis: Beyond traditional donor-acceptor combinations. *Angew. Chem., Int. Ed. 45*, 4562–4588.
45. García-Echeverría, C., and Rich, D. H. (1992) New intramolecularly quenched fluorogenic peptide substrates for the study of the kinetic specificity of papain. *FEBS Lett. 297*, 100–102.
46. Janowski, B., Wöllner, S., Schutkowski, M., and Fischer, G. (1997) A protease-free assay for peptidyl prolyl *cis*/*trans* isomerases using standard peptide substrates. *Anal. Biochem. 252*, 299–307.
47. Zoldák, G., Aumüller, T., Lücke, C., Hritz, J., Oostenbrink, C., Fischer, G., and Schmid, F. X. (2009) A library of fluorescent peptides for exploring the substrate specificities of prolyl isomerases. *Biochemistry 48*, 10423–10436.
48. Chauhan, R., and Mande, S. C. (2002) Site-directed mutagenesis reveals a novel catalytic mechanism of *Mycobacterium tuberculosis* alkylhydroperoxidase C. *Biochem. J. 367*, 255–261.
49. Schiene-Fischer, C., Habazettl, J., Schmid, F. X., and Fischer, G. (2002) The hsp70 chaperone DnaK is a secondary amide peptide bond *cis-trans* isomerase. *Nat. Struct. Biol. 9*, 419–424.
50. Ranganathan, R., Lu, K. P., Hunter, T., and Noel, J. P. (1997) Structural and functional analysis of the mitotic rotamase Pin1 suggests substrate recognition is phosphorylation dependent. *Cell 89*, 875–886.
51. Heikkinen, O., Seppala, R., Tossavainen, H., Heikkinen, S., Koskela, H., Permi, P., and Kilpeläinen, I. (2009) Solution structure of the parvulin-type PPIase domain of *Staphylococcus aureus* PrsA: Implications for the catalytic mechanism of parvulins. *BMC Struct. Biol. 9*, 17.
52. Bailey, M. L., Shilton, B. H., Brandl, C. J., and Litchfield, D. W. (2008) The dual histidine motif in the active site of Pin1 has a structural rather than catalytic role. *Biochemistry 47*, 11481–11489.
53. Daniels, D. L., Plunkett, G., Burland, V., and Blattner, F. R. (1992) Analysis of the *Escherichia coli* genome: DNA sequence of the region from 84.5 to 86.5 minutes. *Science 257*, 771–778.
54. Wood, Z. A., Poole, L. B., and Karplus, A. (2003) Peroxiredoxin evolution and the regulation of hydrogen peroxide signaling. *Science 300*, 650–653.
55. Woo, H. A., Chae, H. Z., Hwang, S. C., Yang, K. S., Kang, S. W., Kim, K., and Rhee, S. G. (2003) Reversing the inactivation of peroxiredoxins caused by cysteine sulfinic acid formation. *Science 300*, 653–656.
56. Malešević, M., Jahreis, G., Wawra, S., Fischer, G., and Lücke, C. (2008) Conformational consequences of regio- and stereoselective disulfide bridge oxidation in a cyclic peptide. *ChemBioChem 9*, 46–49.
57. Poole, L. B., and Ellis, H. R. (1996) Flavin-dependent alkyl hydroperoxide reductase from *Salmonella typhimurium*. 1. Purification and enzymatic activities of overexpressed AhpF and AhpC proteins. *Biochemistry 35*, 56–64.
58. Storz, G., Jacobson, F. S., Tartaglia, L. A., Morgan, R. W., Silveira, L. A., and Ames, B. N. (1989) An alkyl hydroperoxide reductase induced by oxidative stress in *Salmonella typhimurium* and *Escherichia coli*: Genetic characterization and cloning of *ahp*. *J. Bacteriol. 171*, 2049–2055.
59. Trandinh, C. C., Pao, G. M., and Saier, M. H., Jr. (1992) Structural and evolutionary relationships among the immunophilins: Two ubiquitous families of peptidyl-prolyl *cis-trans* isomerases. *FASEB J. 6*, 3410–3420.
60. Hacker, J., and Fischer, G. (1993) Immunophilins: Structure-function relationship and possible role in microbial pathogenicity. *Mol. Microbiol. 10*, 445–456.